Mechanics of Composite Materials, Vol. 45, No. 3, 2009

ASSESSMENT OF TRANSMISSION OF THE SHEAR STRESS IN POTTED ANCHORS FOR COMPOSITE RODS 1. SLEEVE OF CONSTANT THICKNESS

G. G. Portnov,* C. E. Bakis,**
and V. L. Kulakov*

Keywords*: FRP, composite, rod, tendon, anchor, shear stress, analytical model*

The key problem facing the application of fiber-reinforced polymer (FRP) stay cables and tendons is the anchorage. Potted (bond-type) anchors have been used more extensively than anchors of any other type. The main aim in the design of anchors is to minimize the peak shear stress at the FRP rod-pottant interface. To this end, parametric analyses of the stress state in the anchors are carried out. Since parametric studies cannot be easily performed by the finite-element method, an analytical model of the anchor is proposed. The model involves significant simplifying assumptions and allows one to obtain a relatively simple analytical solution for shear-stress distributions at the FRP rod-pottant interface. The use of this solution at various boundary conditions and various geometrical and mechanical parameters of anchor components enables one to search for and evaluate, at least qualitatively, different methods for decreasing the peak interfacial shear stress in the anchor. In this part of the investigation, an anchor consisting of a sleeve of constant thickness is considered.

Introduction

Owing to the good corrosion resistance, high strength, and advantageous strength-to-weight ratio, pultruded fiber-reinforced polymer (FRP) composites have a potential to outperform steel tendons in a variety of construction applications in civil and mining engineering. For example, FRP tendons and cables are used as suspension and stay cables for bridges and for strengthening and rehabilitation of existing structures [1, 2]. Furthermore, FRP tendons have been employed to create support systems in underground infrastructures [3] and to reinforce masonry walls, railway sleepers, pontoons, barges, and other special structures [4-7].

The key problem to which the application of stay cables and tendons is faced is the anchorage. The low ratios of the lateral compressive strength and the longitudinal shear strength to the longitudinal tensile strength of FRP tendons create a challenge for the present anchorage techniques. For instance, the conventional steel wedge/sleeve anchors used for steel tendons do not create a favorable load transfer situation, resulting in premature failure of the FRP material in the anchorage zone.

---

* Institute of Polymer Mechanics, University of Latvia, Riga, Latvia. ** Department of Engineering Science & Mechanics, The Pennsylvania State University, University Park, PA, USA. Russian tanslation published in Mekhanika Kompozitnykh Materialov, Vol. 45, No. 3, pp. 321-346, May-June, 2009. Original article submitted September 12, 2008.

0191-5665/09/4503-0217

Thus far, many anchorage systems have been developed for FRP tendons. They can be classified into three types: clamp (friction) anchors, potted (bonded) anchors, and wedge (self-tightening friction) anchors [8, 9]. Potted anchors have been used more extensively than anchors of any other type. A potted anchor consists of a metallic or nonmetallic sleeve inside of which single or multiple tendons or rods are bonded with a pottant. The sleeve can be anchored with a bearing nut or can bear directly on the element being prestressed. The pottant can be a polymer-based adhesive (usually epoxy), a low-temperature melting metallic material, or a cementitious material [4]. Potted anchors can be suitable for all types of FRP tendons [4], and they are most commonly used for post-tensioning applications [8-13]. Cylindrical sleeves are simple to manufacture, and their quality is easy to control.

The optimal design of anchors aims to realize the maximum tensile strength of the rod-like FRP material. Considering steel tendons, the maximum strength is reached when the failure occurs within the free length of the tendon, that is, when the anchorage has no detrimental influence. A highly anisotropic material, such as a pultruded FRP rod with fibers entirely or predominantly in the longitudinal direction, shows a different behavior: this material most often fails within or near the anchorage area. The main reason for such a behavior is the sensitivity of the FRP rod to the manner of its loading by the anchor. The transfer of forces across the interface by the bond between the pottant and FRP rod is of fundamental importance in many aspects of anchorage design. If a force is applied to the outside of the sleeve, it will be transferred to the rod through the sleeve-pottant and pottant-rod interfaces, causing nonuniform tensile stresses in the rod and shear stresses in the pottant along the anchor length. The longitudinal shear stresses reach a peak magnitude at the loaded or inner end of the anchor. The peak shear stress must be lower than the bond strength of the interface and the cohesive strength of the pottant in order to prevent pull-out of the rod. Also, it must be lower than the longitudinal shear strength of the FRP material to prevent failure of the rod. However, even if the maximum shear stress is lower than the shear strength of the FRP rod, it can still cause failure of the rod due to the concentration of longitudinal tensile stresses at the surface of the rod at the position of the peak interfacial shear stress [14]. Therefore, the lowering of the peak interfacial shear stress is one of the main aims in the design of anchorages for FRP rods. The present paper is dedicated to the assessment of the influence of various material and geometric parameters of potted anchors for round FRP rods on the peak shear stress at the interface between the pottant and rod.

1. Problem Statement

The transfer of forces across the interface by the bond between the pottant and the FRP rod is of fundamental importance in many aspects of FRP anchorages for post-tensioned applications. It should be mentioned that similar problems connected with transfer of tensile loads to cylindrical bearing elements have also been considered in other areas. For example, such problems are considered in the mechanics of composites: fiber/matrix stress transfer [15], stress concentration in unidirectional composites near a broken fiber [16], and the analysis of the "pull-out" test for a single fiber [17, 18]. The so-called "shear-lag" analysis is used in all these studies. The shear-lag analysis as a tool for a stress analysis in composite materials is usually traced back to Cox [19]. A detailed analysis of the shear-lag method and a review of papers connected with the use of this method are presented in [20]. The most fundamental mathematical assumption of shear-lag analysis requires that, in axisymmetric problems, the variation in the radial displacement u with respect to the axial coordinate z is zero or negligible, $u/z \approx 0$. This assumption will also be used in the model considered in the present work. The shear-lag equations are usually easily solved. When a shear-lag analysis is performed correctly, the results obtained are quite accurate.

The same approach was used by R. Tepfers [21], who developed a mathematical model able to predict the bond stress and the stresses in lap-spliced reinforcing bars and in the surrounding concrete. The governing equations in this case are very close to those considered in the present study.

Another group of problems that are close to the problem considered in this paper concerns adhesive tubular lap joints, where the tensile load is transferred from one thin tubular shell to another through a thin adhesive layer [22-24]. In [22], the adherends were investigated by means of the ordinary theory of bending and stretching of thin isotropic shells. The governing system of high-order linear ordinary differential equations with constant coefficients was solved numerically. In [23, 24], the finite-element method (FEM) was used for stress-state calculations, and both shear and peel stresses were determined. In the

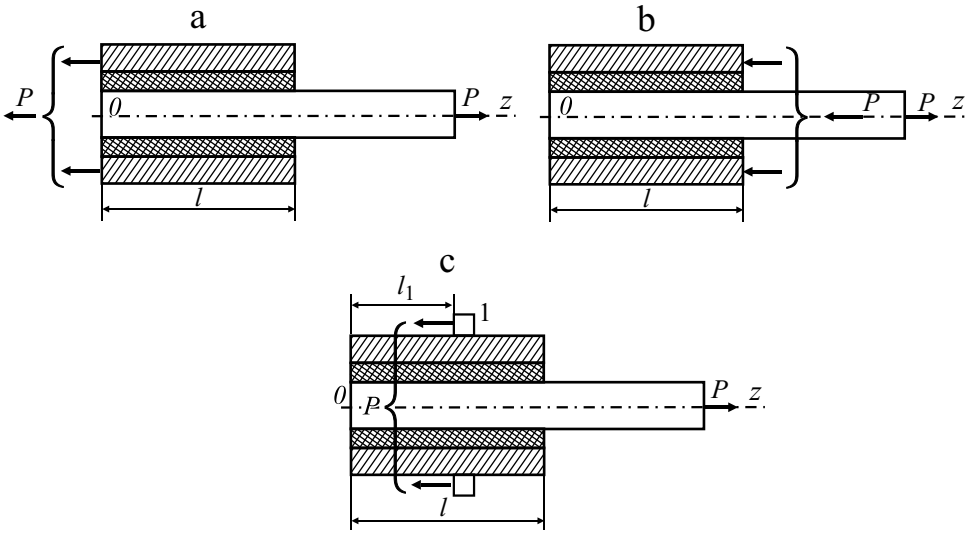

Fig. 1. Loading schemes (1, 2, and 3) considered: a tensile force at $z = 0$ (a); a compressive force at $z \quad l$ (b); an arbitrary location of the load point (c). 1 — locknut.

examples considered, it was shown that, at high ratios between the elastic moduli of the adherend and adhesive, the peel stresses are more than four times lower than the shear stresses.

The subject of inquiry in the present study is, in a sense, simpler than those addressed in the above-mentioned papers. A potted anchor consists of a round, solid FRP rod surrounded by a thick layer of pottant enclosed in a thick sleeve. In models considering the interaction between the rod and matrix, the outer effective radius of the matrix cylinder is defined as the radius beyond which the rod does not affect the deformation of the matrix. This radius can depend on the acting load. In contrast to such models, the outer radius of a potted anchor is fixed. In comparison with the tubular joints mentioned, the joining elements (sleeve and rod) are thick and have a high curvature, which prevents their axial bending and allows one to neglect the peel stresses. Therefore, the problem of load transfer in a potted anchor is more definite and sometimes simpler than the problems considered in the above-mentioned publications.

The analysis of stresses in potted anchors is usually carried out by the FEM [25, 26]. The calculations have shown that the distribution of stresses in the pottant is highly dependent on the anchor construction and material properties. But parametric studies cannot be easily performed by using the FEM. Therefore, there is a need for analytical models, calibrated to experimental results, upon which a rational approach to the design of FRP potted anchorage systems can be based. Such a model is proposed in the present study. It involves significant simplifying assumptions and gives an opportunity to obtain a relatively simple analytical solution for shear-stress distributions at the FRP rod-pottant interface. The use of this solution, at various boundary conditions and different geometrical and mechanical parameters of anchor components, enables one to search for and evaluate, at least qualitatively, different means of decreasing the peak interfacial shear stress in the anchor and of increasing the tensile load-carrying capacity.

2. Theoretical Analysis

2.1. Description of the model. It is suggested to simulate the potted (bond-type) anchorage for round composite rods with a simple model. The system to be modeled consists of an inner cylindrical FRP rod, an intermediate cylindrical layer, and an outer sleeve, connected with each other in a way excluding slipping and loaded in tension. The materials of all the components are linearly elastic. External forces P are applied to either of sleeve ends and to the loaded end of the rod (Fig. 1a, b). The analysis is based on the hypotheses that (i) the stress states in the rod and sleeve are one-dimensional, (ii) plane cross sections in the rod and sleeve remain plane after loading, and (iii) the intermediate cylindrical layer is loaded only in shear and is not subjected to tensile and peel stresses. The aim is to estimate the shear stresses at interfaces of the cylinders. The validity of this

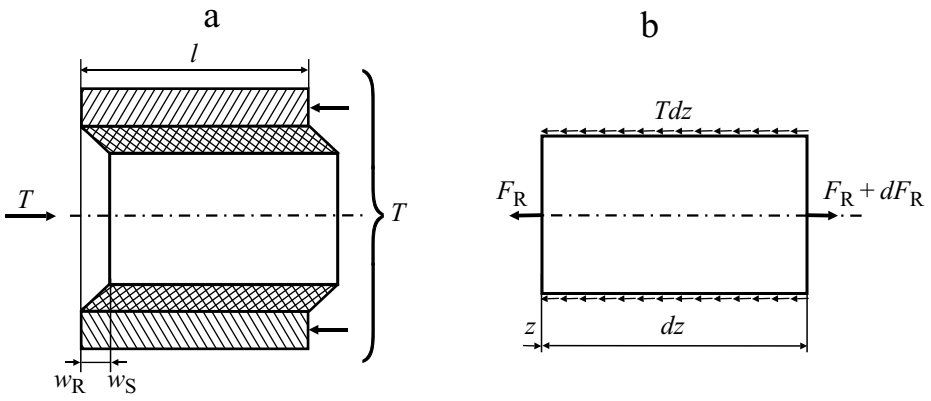

Fig. 2. Loading scheme of the cylindrical differential element of a FRP rod.

model will be verified by solving the problem with the use of FEM. Hereafter, the subscripts R, I, and S will refer to the inner cylindrical rod, the intermediate potted layer, and the outer sleeve, respectively.

The problem statement is partly similar to that presented in [8], where the outer sleeve was assumed to be perfectly rigid. This study contains a discrepancy connected with the assumption that the axial displacement of the outer rigid sleeve is equal to zero. This simplification is unnecessary, and, as will be seen later, a more accurate problem statement does not cause considerable difficulties.

Let us assume that the shear force per unit length, T, acting on the outer surface of unit length of the inner rod and on the inner surface of the sleeve is proportional to the relative displacement of the rod and sleeve:

$$T \quad k(w_R \quad w_S), \tag{1}$$

where k is a coefficient, which can be determined theoretically (as will be shown later) or experimentally; $(w_R \quad w_S)$ is the relative axial displacement of the rod and sleeve caused by their elongation and by shear deformation of the intermediate layer.

Considering the balance of forces acting on a small element of the rod (Fig. 2), we can write that

$$\frac{dF_R}{dz} \quad T, \tag{2}$$

where z is defined as shown in Fig. 1b. The differentiation of Eq. (1) gives

$$\frac{dT}{dz} \quad k\,\frac{dw_R}{dz} \quad \frac{dw_S}{dz} \quad . \tag{3}$$

The axial displacements of the rod and sleeve are related to tensile stresses by Hooke's law:

$$\frac{dw_R}{dz} \quad R \quad \frac{F_R}{E_R S_R}, \quad \frac{dw_S}{dz} \quad S \quad \frac{F_S}{E_S S_S}. \tag{4}$$

In Eqs. (4), $F_{R,S}$, $E_{R,S}$, and $S_{R,S}$ are the normal forces, the moduli of elasticity, and cross-sectional areas of the rod and sleeve, respectively. Substituting Eq. (2) into Eq. (3), we obtain

$$\frac{d^2F_R}{dz^2} \quad k\,\frac{F_R}{E_R S_R} \quad \frac{F_S}{E_S S_S} \quad . \tag{5}$$

2.2. An external force applied to the outer end of the sleeve. For loading conditions corresponding to Fig. 1a, the equation of total balance of forces has the form

$$F_S \quad F_R \quad P. \tag{6}$$

From Eqs. (5) and (6), it follows that

$$\frac{d^2 F_R}{dz^2} \quad {}^2 F_R \quad k \frac{P}{E_S S_S}, \tag{7}$$

where

$${}^2 \quad k \left(\frac{1}{E_R S_R} \quad \frac{1}{E_S S_S} \right). \tag{8}$$

Equation (7) is very similar to the governing equation occurring in all studies on the mechanics of composites using the shear-lag analysis (see the above-mentioned papers). The main differences are in the value of the shear-lag parameter and in the coefficient on the right-hand side of the equation. Adding up the general solution of the corresponding homogeneous equation and a particular solution of Eq. (7), we obtain the expression for F_R

$$F_R \quad A \sinh(\quad z) \quad B \cosh(\quad z) \quad \frac{kP}{{}^2 E_S S_S}, \tag{9}$$

and using Eq. (2), the expression for T

$$T \quad \frac{dF_R}{dz} \quad A \quad \cosh(\quad z) \quad B \quad \sinh(\quad z). \tag{10}$$

The constants A and B are found from the boundary conditions

$$F_R \quad 0 \text{ at } z \quad 0, \quad F_R \quad P \text{ at } z \quad l. \tag{11}$$

After solving system (11), we obtain

$$A \quad \frac{kP}{{}^2 E_S S_S} \frac{1 \quad \cosh(\quad l)}{\sinh(\quad l)} \quad \frac{P}{\sinh(\quad l)}, \quad B \quad \frac{kP}{{}^2 E_S S_S}.$$

The longitudinal normal force (9) in the rod now is expressed as

$$F_R \quad \frac{P}{1} \quad \frac{1}{\sinh(\quad l)} [\quad (\sinh(\quad l) \quad \sinh(\quad (l \quad z))) \quad \sinh(\quad z)],$$

where $\frac{E_R S_R}{E_S S_S}$.

The longitudinal normal force in the sleeve is

$$F_S \quad P \quad F_R \; T \quad \frac{dF_R}{dz} \quad A \quad \cosh(\quad z) \quad B \quad \sinh(\quad z).$$

The shear force per unit length in the intermediate layer is

$$T \quad \frac{dF_R}{dz} \quad \frac{P}{1} \quad \frac{}{\sinh(\quad l)} [\quad \cosh(\quad (l \quad z)) \quad \cosh(\quad z)]. \tag{12}$$

2.3. An external force applied to the inner end of the sleeve. Let us consider the case where a compressive force is applied to the inner end $z \quad l$ of the sleeve (Fig. 1b). It this case, equilibrium equation (6) for the contact region reads

$$F_S \quad F_R \quad 0, \tag{13}$$

and Eq. (7) becomes homogeneous:

$$\frac{d^2F_R}{dz^2} \quad {}^2F_R \quad 0. \tag{14}$$

The solution of Eq. (14) has the form

$$F_R \quad A\sinh(\ z) \quad B\cosh(\ z). \tag{15}$$

The shear force is determined as before:

$$T \quad \frac{dF_R}{dz} \quad A \quad \cosh(\ z) \quad B \quad \sinh(\ z). \tag{16}$$

The constants A and B, found from boundary conditions (11), have the values

$$A \quad \frac{P}{\sinh(\ l)}, \quad B \quad 0.$$

The longitudinal normal and shear forces are calculated using Eqs. (4), (5), and (13):

$$F_R \quad P\frac{\sinh(\ z)}{\sinh(\ l)}, \quad T \quad P \quad \frac{\cosh(\ z)}{\sinh(\ l)}, \quad F_S \quad F_R. \tag{17}$$

The relations for the tensile force F_R and shear force per unit length, T, in the general form (9), (10) or (15), (16) will be used in various design models in the following analysis.

2.4. Arbitrary location of the load point. The results obtained may be used to clarify the effect of location of the load point along the sleeve of constant thickness on the stress state in the anchor. Such a variable load point $z \quad l_1$ (see Fig. 1c) can be realized, for example, through a locking bearing nut moving along the thread on the surface of the sleeve.

In this case, the solution on the interval $0 \quad z \quad l_1$ is similar to (15), (16):

$$F_{R1} \quad A_1\sinh(\ z) \quad B_1\cosh(\ z), \tag{18}$$

$$T_1 \quad A_1 \quad \cosh(\ z) \quad B_1 \quad \sinh(\ z).$$

The form of solution on the interval $l_1 \quad z \quad l$ is similar to (9), (10):

$$F_{R2} \quad A_2\sinh(\ z) \quad B_2\cosh(\ z) \quad \frac{kP}{{}^2E_SS_S}, \tag{19}$$

$$T_2 \quad A_2 \quad \cosh(\ z) \quad B_2 \quad \sinh(\ z).$$

The boundary conditions are

$$F_{R1} \quad 0 \text{ at } z \quad 0, \quad F_{R1} \quad F_{R2} \text{ at } z \quad l_1, \tag{20}$$

$$\frac{dF_{R1}}{dz} \quad \frac{dF_{R2}}{dz}(T_1 \quad T_2) \text{ at } z \quad l_1, \quad F_{R2} \quad P \text{ at } z \quad l.$$

The third condition in (20) is the result of continuity of the longitudinal displacement at the point $z \quad l_1$ and of homogeneity of the intermediate cylinder. Since $w_{Sl} \quad w_{S2}$ and $w_{R1} \quad w_{R2}$, $w_{R1} \quad w_{Sl} \quad w_{R2} \quad w_{S2}$ and $T_1 \quad T_2$ [see Eq. (1)], and therefore $\frac{dF_{R1}}{dz} \quad \frac{F_{R2}}{dz}$ [see Eq. (2)].

After substituting relations (18) and (19) for F_{R1} and F_{R2} into Eq. (20) and solving the system of equations, we obtain the following relations for shear forces in the intermediate cylinder and, using Eqs. (6) and (17), for the normal forces F_{Sl} and F_{S2} in the sleeve when an external force P is applied to the sleeve at the point $z \quad l_1$:

$$T_1 \quad \frac{P \quad \cosh(\quad z)[\quad \cosh(\quad l \quad l_1)) \quad 1]}{(1 \quad)\sinh(\quad l)} \quad (0 \quad z \quad l_1), \tag{21}$$

$$T_2 \quad \frac{P \quad [\quad \cosh(\quad l \quad)\cosh(\quad (l \quad z)) \quad \cosh(\quad z)]}{(1 \quad)\sinh(\quad l)} \quad (l_1 \quad z \quad l), \tag{22}$$

$$F_{Sl} \quad \frac{P\sinh(\quad z)[\quad \cosh(\quad l \quad l_1)) \quad 1]}{(1 \quad)\sinh(\quad l)} \quad (0 \quad z \quad l_1), \tag{23}$$

$$F_{S2} \quad \frac{P}{(1 \quad)\cosh(\quad l)} \quad \cosh(\quad l) \quad \cosh(\quad z) \quad \frac{[\quad \cosh(\quad l)\cosh(\quad l_1) \quad 1]\sinh(\quad (l \quad z))}{\sinh(\quad l)}$$

$$(l_1 \quad z \quad l). \tag{24}$$

2.5. Simulating the shear stiffness of the intermediate (potted) cylinder. Before analyzing the results obtained, it is necessary to examine the governing parameters of the problem more carefully. Let us consider the intermediate potted cylinder to estimate the value of k in Eq. (1) theoretically. For approximation of this parameter, we will examine the stress state of a thick infinitely long hollow cylinder loaded with constant shear stresses $_0$ and $_i$ at its outer and inner surfaces, respectively; the stress $_i$ is aligned with the positive direction of the z-axis, but $_0$ has the opposite direction. In our case, the shear stresses satisfy the requirement $_0 r_0 \quad _i r_i$, i.e., the cylinder is not loaded with a longitudinal normal force. This type of loading was also considered in [26, 27] by using stress functions of a particular type. Employing the results of these studies and taking into account that $T \quad _i 2 \quad r_i$, we obtain the simple relation

$$k \quad \frac{2 \quad G_I}{\ln(r_0/r_i)},$$

where $G_I \quad \frac{E_I}{2(1 \quad _I)}$ is the elastic shear modulus of the intermediate potted cylinder. This expression for k must be inserted into relation (8). Introducing the dimensionless parameter $^- \quad l$ and variable $\bar{z} \quad z/l$, we have

$$-2 \quad l^2 k \quad \frac{1}{E_R S_R} \quad \frac{1}{E_S S_S} \quad \frac{G_I}{E_R} \quad \frac{2}{\ln(r_0/r_i)} \quad \frac{l^2}{S_R}(1 \quad) \quad \frac{G_I}{E_R} \quad \frac{2(1 \quad)}{\ln(r_0/r_i)} \quad \frac{l^2}{r_R^2},$$

where $\frac{E_R S_R}{E_S S_S}$, and $r_i \quad r_R$ is the radius of the rod.

Using the additional dimensionless parameters $_E \quad G_I/E_R$, $_r \quad r_0/r_i$, and $_L \quad l/r_R$, we finally arrive at the relation for $^-$ in the form

$$- \quad L\sqrt{\frac{2 \quad E}{\ln \quad _r}(1 \quad)}, \tag{25}$$

which will be used in all subsequent calculations and analyses.

3. Parametric Analysis

3.1. Analytical study. In accordance with the aim of this investigation, let us analyze the interfacial shear stresses. We normalize the shear stress $_R \quad \frac{T}{2\ R}$ at the surface of FRP rod to the mean tensile stress in the rod $_{mR} \quad \frac{P}{R^2}$ in its fully loaded part, namely $^{-}_R(z) \quad \frac{_R(z)}{_{mR}}$. The relation corresponding to loading of the sleeve according to scheme 1 (Fig. 1a), where an external tensile load is applied to its outer end [normalized relation (12)], has the form

$$^{-}_{R1}(\bar{z}) \quad \frac{1}{2\ _L}\ \frac{1}{1}\ \frac{^{-}}{\sinh(^{-})}[\ \cosh(^{-}(1\ \ \bar{z}))\ \ \cosh(^{-}\bar{z})]. \tag{26}$$

If an external compressive force is applied to the inner end of the sleeve (scheme 2, Fig. 1b), then

$$^{-}_{R2}(\bar{z}) \quad \frac{1}{2\ _L} - \frac{\cosh(^{-}\bar{z})}{\sinh(^{-})}. \tag{27}$$

First, let us analyze scheme 1 and compare shear stresses at the inner ($\bar{z}$ 1) and outer ($\bar{z}$ 0) ends of the rod inside the anchor. The difference between these stresses is

$$^{-}_{R1}(1)\ \ ^{-}_{R1}(0) \quad \frac{1}{2\ _L}\ \frac{1}{1}\ \frac{^{-}}{\sinh(^{-})}(\ \ 1)(1\ \ \cosh(^{-})). \tag{28}$$

As may be seen from Eq. (28), $^{-}_{R1}(1)\ \ ^{-}_{R1}(0)\ \ 0$ if 1 (the rod is stiffer than the sleeve in tension). If 1 (the sleeve is stiffer in tension), $^{-}_{R1}(1)\ \ ^{-}_{R1}(0)\ \ 0$. If the tensile stiffnesses of the sleeve and rod are the same (= 1), the shear stresses at both ends of the rod are equal (the most favorable situation). Thus, the ratio of rod and sleeve stiffnesses plays an important role in the distribution of shear stresses at the rod surface.

Substituting expression (25) for $^{-}$ in the numerator of Eq. (26), we obtain

$$^{-}_{R1}(\bar{z}) \quad \frac{1}{2}\ \frac{1}{1}\ \frac{\sqrt{\frac{2\ _E}{\ln\ _r}(1\ \ )}}{\sinh(^{-})}[\ \cosh(^{-}(1\ \ \bar{z}))\ \ \cosh(^{-}\bar{z})].$$

If $_L$, then $^{-}$, and we see that the maximum value of $^{-}_R$ remains limited when the length of anchor l grows infinitely. At 1 (a stiff sleeve), the maximum shear stress occurs at $\bar{z}$ 1 and

$$^{-}_{R1}(1) \quad \frac{1}{2}\ \frac{1}{1}\sqrt{\frac{2\ _E}{\ln\ _r}(1\ \ )}\ \frac{}{\sinh(^{-})}\coth^{-} \ - \qquad \frac{1}{2}\ \frac{1}{1}\sqrt{\frac{2\ _E}{\ln\ _r}(1\ \ )}.$$

At 1 (a soft sleeve), the shear stresses are maximum at $\bar{z}$ 0 and

$$^{-}_{R1}(0) \quad \frac{1}{2}\ \frac{1}{1}\sqrt{\frac{2\ _E}{\ln\ _r}(1\ \ )}\ \ \coth^{-}\ \ \frac{1}{\sinh(^{-})} - \qquad \frac{1}{2}\ \frac{1}{1}\sqrt{\frac{2\ _E}{\ln\ _r}(1\ \ )}.$$

Now, let us turn to scheme 2, where a compressive longitudinal force is applied to the inner end of the sleeve. It is evident [see Eq. (27)] that the shear stress is maximum near the force point $\bar{z} = 1$. It is interesting to compare the maximum shear stresses for both the loading schemes, assuming that all other parameters of the system are the same. If 1,

$$\frac{^{-}_{R2}(1)}{^{-}_{R1}(0)} \quad \frac{(\ \ 1)}{\frac{1}{\cosh^{-}}} \quad 1. \tag{29}$$

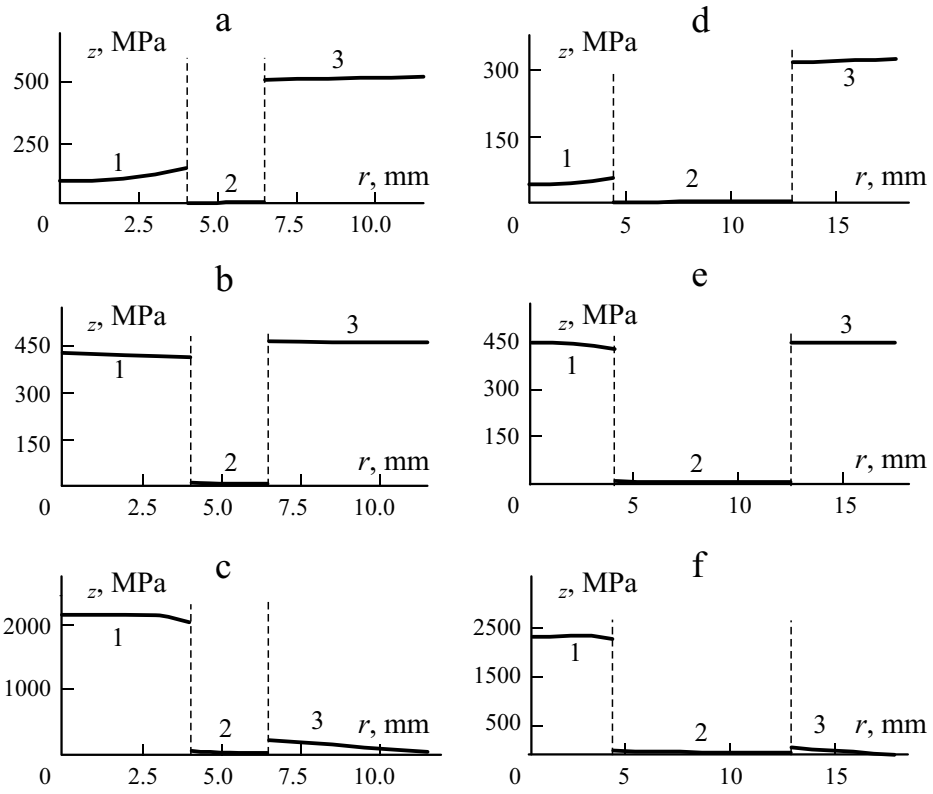

Fig. 3. Tensile stresses $_z$ vs. radius r for the CFRP rod (1), epoxy pottant (2), and steel sleeve (3) in anchor cross sections at z = 0.01 (a, d), 0.158 (b, e), and 0.241 m (c, f) and at thicknesses of the potted cylinder equal to 2.5 (a, b, c) and 8.5 mm (d, e, f) under loading according to scheme 1 (Fig. 1a).

If l,

$$\frac{\bar{}_{R2}(1)}{\bar{}_{R1}(1)} \quad \frac{(\quad 1)}{\cosh \bar{}} \quad 1. \tag{30}$$

As may be seen from Eqs. (29) and (30), for all values of the parameter (the ratio of tensile stiffnesses of the rod and sleeve), the maximum shear stress is always higher in the loading scheme where the external force is applied to the inner end of the sleeve (scheme 2).

If the tensile stiffness of the sleeve is infinitely high (0), expressions of shear stresses, (26) and (27), for schemes 1 and 2 coincide. As would be expected, the location of the external force applied to a rigid sleeve has no effect on the distribution of shear stresses in the intermediate cylinder. Ratio (30) is equal to unity, and the maximum shear stress (at $\bar{z} = 1$) is given by the expression

$$\bar{}_{R1}(1) \quad \bar{}_{R2}(1) \quad \frac{1}{2}\sqrt{\frac{2 \quad E}{\ln \quad r}} \coth(\bar{}).$$

3.2. Numerical study. First, let us consider the results calculated by the FEM. The analytical model presented involves significant simplifying assumptions. To evaluate the accuracy of shear stresses calculated by the model proposed, the stress state in the anchor was calculated by means of the FEM. Owing to symmetry of the problem, it suffices to model only one quadrant of the anchor configuration. External forces were applied to a cross section of the composite rod far from the anchor-

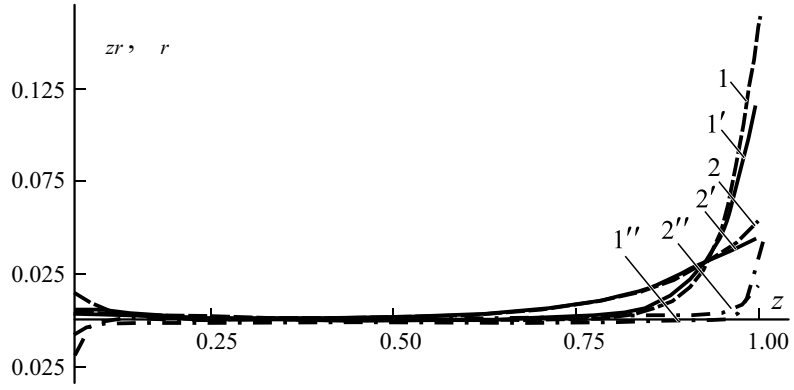

Fig. 4. Distributions of the relative interfacial shear stress $\bar{}_{zr}$ (1 and 2 — closed-form solution; 1 and 2 — FEM) and the interfacial radial (peel) stress $\bar{}_{r}$ (1 and 2 ' — FEM) along the anchorage zone z in the anchor for the CFRP rod with a cementitious grout (1) and an epoxy pottant (2).

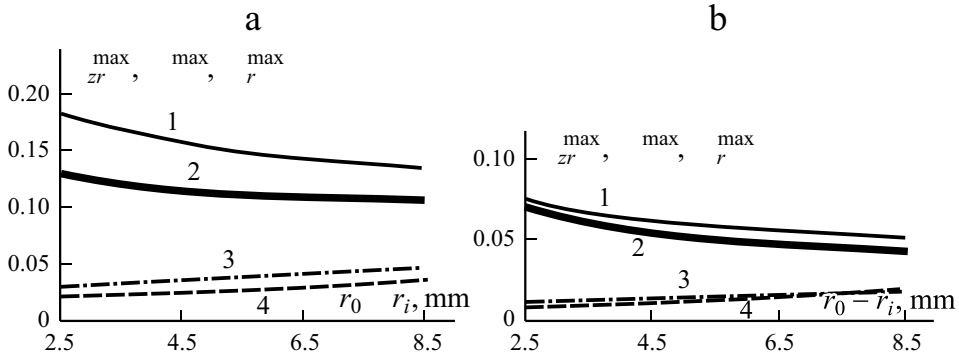

Fig. 5. The maximum relative shear stress $\bar{}^{\max}_{zr}$ (1 — closed-form solution; 2 — FEM), hoop stress $\bar{}^{\max}$ (3 — FEM), and radial stresses $\bar{}^{\max}_{r}$ (4 — FEM) vs. the thickness (r_0 r_i) of intermediate cylinders consisting of a cementitious grout (a) and an epoxy pottant (b).

age zone and to the outer end of the sleeve (scheme 1, Fig. 1a). The FEM program used three-dimensional 8-node isoparametric elements.

The values of geometrical and material parameters were as follows: radius of the FRP rod $r_{\mathrm{R}} = 0.004$ m; radii of the sleeve $r_{\mathrm{si}} = 0.0065$ and 0.0125; $r_{\mathrm{so}} = 0.0175$ m; length of the anchor $l = 0.250$ m; length of the rod outside the anchor, $l_{\mathrm{free}} = 0.100$ m.

The mechanical properties of anchor components were as follows. Carbon FRP rod (IM7/3501-6): $E_z = 160$ GPa, E_r E = 10 GPa, G_{zr} G_z = 5 GPa, G_r = 3 GPa, $_{zr}$ $_z$ = 0.01875, and $_r$ = 0.52. Steel sleeve: $E = 200$ GPa and $_{\mathrm{S}}$ 0.35. Potted cylinder: $E = 3$ GPa, = 0.30 (epoxy pottant), $E = 26$ GPa, and = 0.22 (cementitious grout).

Distributions of the longitudinal tensile stress in the carbon FRP rod, epoxy-potted cylinder, and steel sleeve are presented in Fig. 3. As may be seen, they are practically uniform, and the tensile stresses in the pottant are very small. Thus, the resultant longitudinal forces in the intermediate cylinder are very close to zero, and the use of equilibrium equations (6) and (13) is justified. These results confirm the validity of the assumptions made in Sect. 2.1.

A comparison of distributions of the normalized (related to the mean tensile stresses in the rod) interfacial shear and peel stresses obtained by both the methods are presented in Fig. 4, where the distributions are displayed only to the point 1 mm distant from the inner end of the potted cylinder to avoid singularities. The maximum normalized stresses in relation to the

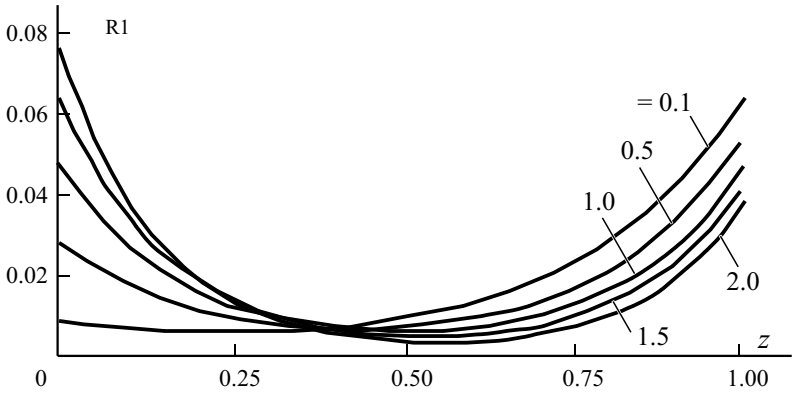

Fig. 6. Shear-stress distribution between the rod and the intermediate cylinder for different values of . Loading scheme 1. $_L = 30$, $_r = 3.125$, and $_E = 0.01$.

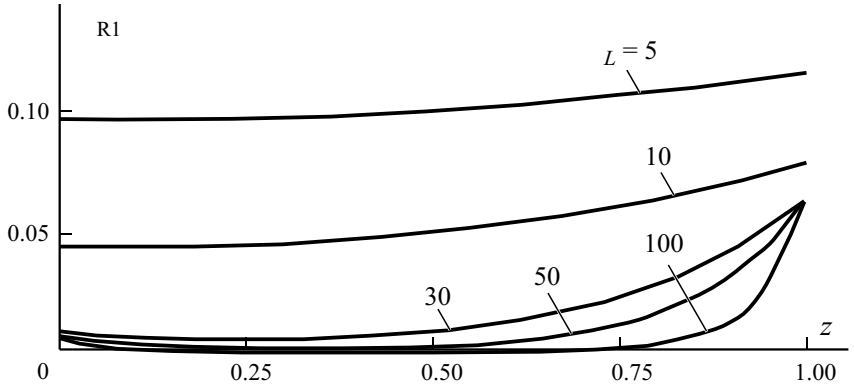

Fig. 7. Shear-stress distribution between the rod and the intermediate cylinder for different relative lengths $_L$ of the anchor. Loading scheme 1. = 0.1, $_r = 3.125$, and $_E = 0.01$.

thickness of the potted cylinder are shown in Fig. 5. A comparison shows a good agreement between the solutions for shear stresses given by the closed-form theory and the FEM models; the hoop and peel stresses are several times lower than the shear stress and are not critical from the viewpoint of load-carrying capacity. This conclusion is true practically for the entire volume of the intermediate cylinder, except for a narrow zone near its inner edge. The stress state in this zone falls into the category called the end effect, which is one of the most fundamental problems in the mechanics of adhesive joints [23, 29]. The determination of stress concentrations at the edge of a bonded cylinder is difficult even when the FEM is used and calls for finite elements of a special type [30, 31], particularly if the bonded cylinder has a square end, as in our case. This problem is beyond the scope of our paper. Let us only remark that none of the analytical solutions known can accurately describe the stress state in this zone. In practice, the unavoidable presence of a fillet at the end of the potted (bond-type) cylinder modifies the stress distribution and decreases the stress concentration in the edge zone.

Thus, the assumptions accepted do not lead to qualitative differences between the shear-stress distributions calculated by the FEM and the model suggested. Therefore, the relations obtained can undoubtedly be used for evaluating, at least qualitatively, the influence of potted anchor parameters on the peak interfacial shear stress.

A wide spectrum of materials may be chosen for components of the anchorage system: steel, brass, stainless steel, wound FRP, cement tubes wrapped with CFRP, and corrugated steel tubes for the sleeve, polyester, epoxy, expansive cementitious materials for the pottant, and carbon, aramid, or glass FRP for the composite rod. Taking into account such a vari-

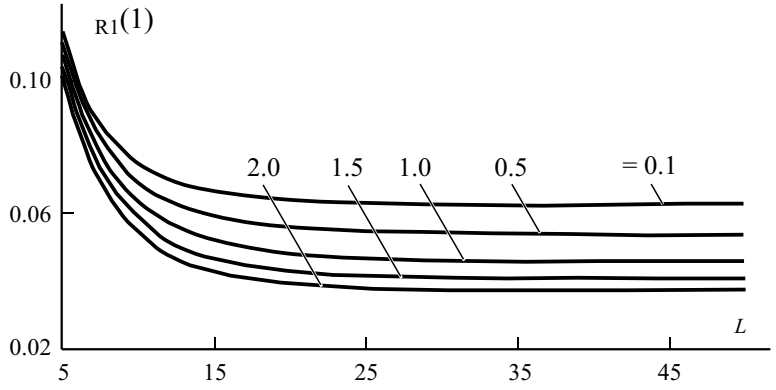

Fig. 8. Shear stresses between the rod and the intermediate cylinder near the loaded end of anchor ($\bar{z}$ l) vs. the relative length $_L$ of the anchor for different values of . Loading scheme 1. $_r$ = 3.125 and $_E$ = 0.01.

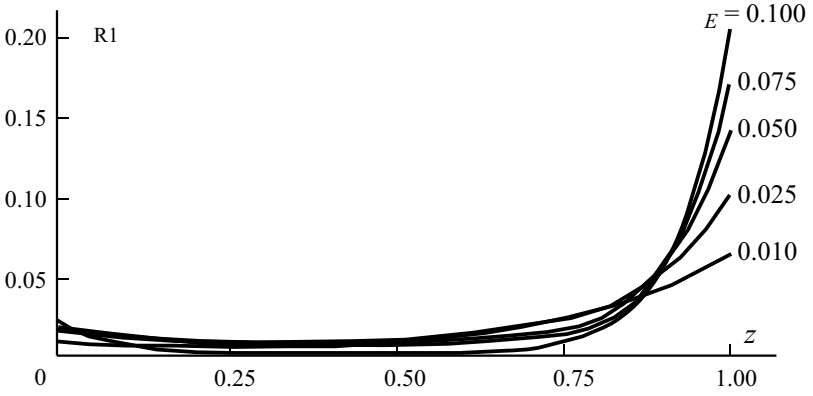

Fig. 9. Shear stresses between the rod and the intermediate cylinder vs. the relative coordinate $\bar{z}$ for different values of $_E$. Loading scheme 1. = 0.1, $_r$ = 3.125, and $_L$ = 30.

ety of materials and their possible combinations, the following basic values of parameters were chosen: $\frac{E_R S_R}{E_S S_S} = 0.1, 0.5,$ 1.0; $_E$ $\frac{G_I}{E_R} = 0.01, 0.1$. The geometrical parameters corresponded to the anchor considered in [10]:

$$_L \quad l/r_R = 30; \quad _r \quad r_0/r_i \quad r_0/r_R = 3.125.$$

First, let us consider the tensile loading of the sleeve at its outer end (scheme 1, Fig. 1a). It is suggested initially that the compliances of the outer sleeve and the intermediate bond cylinder can be varied over a sufficiently wide range. The following results were obtained using relation (26). The impact of the sleeve stiffness in tension on the shear-stress distribution at the interface between the rod and the intermediate cylinder is illustrated in Fig. 6. The results obtained confirm the conclusions drawn from the theoretical analysis. That is, if the stiffness of the sleeve decreases (increases), the shear stress near the inner end ($\bar{z} = 1$) decreases. At = 1, the shear stresses at both ends of the anchorage zone are equal. At l, the maximum value of the shear stress is shifted from $\bar{z} = 1$ to $\bar{z} = 0$. The use of compliant sleeves is generally more favorable for increasing the load-carrying capacity of a bonded anchor in loading scheme 1, because the decreased values of the peak shear stress at the inner end of the rod decrease the concentration of the longitudinal normal stress in cross sections near the point $\bar{z} = 1$ [14]. However, the design of a sleeve more compliant than the tendon involves a problem. Since the sleeve must have a higher tensile

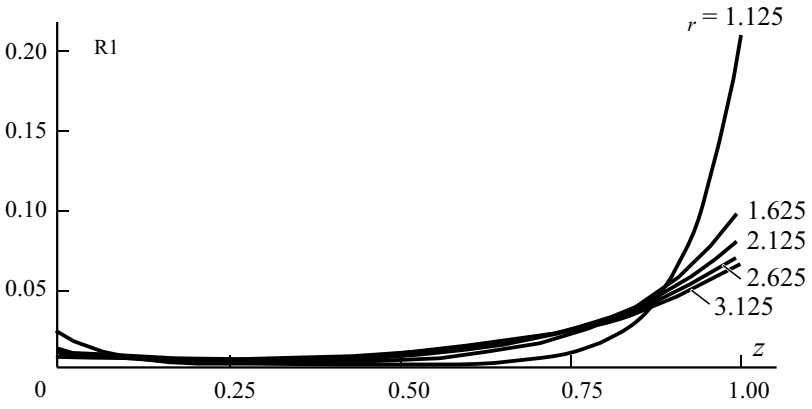

Fig. 10. Shear stresses between the rod and the intermediate cylinder vs. the relative coordinate $\bar{z}$ for different ratios $_r$ between the outer and inner radii of the intermediate potted cylinder. Loading scheme 1. = 0.1, $_L$ = 30, and $_E$ = 0.01.

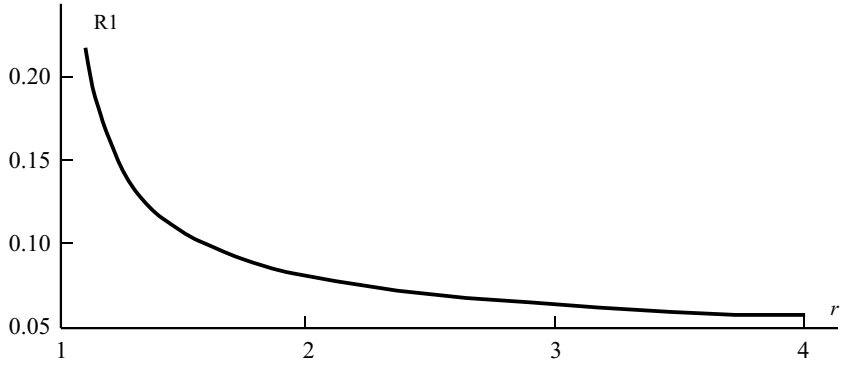

Fig. 11. Shear stresses between the rod and the intermediate cylinder near the inner end of anchor vs. the value of $_r$. Loading scheme 1. $_L$ = 30, = 0.1, and $_E$ = 0.01.

load-carrying capacity than the tendon, it must be made of a strong material, usually with a high modulus of elasticity, or have a large cross-sectional area. It is possible that such contradictory requirements (high strength and low compliance) may be realized by using special sleeves made of a low-modulus, high-strength CFRP or sleeves whose low compliance is achieved by structural means.

Other ways of decreasing the peak shear stress in the rod are connected with increasing the anchor length or with increasing the thickness and shear compliance of the intermediate cylinder. The influence of anchor length in the case of a stiff sleeve (= 0.1) is illustrated in Fig. 7. Lengthening the anchor decreases the peak shear stress to a certain limit, as was predicted by the previous theoretical analysis. This limit is seen more clearly in Fig. 8. Practically, for all values of , variations in the shear stress at $\bar{z}$ = 1 terminate at $_L$ 25-30. Therefore, if the intermediate pottant cylinder is made of a linearly elastic material, very long anchors have no advantage: no further reduction in the peak shear stress at the inner end of the rod can be obtained after reaching a certain critical length (this situation is similar to that in adhesive joints [29] and has also been observed in the context of aramid-FRP prestressed tendons with steel sleeves and a cementitious grout [32]).

A more effective means of reducing the peak shear stress in the FRP rod is to reduce the shear modulus of the intermediate potted cylinder (Fig. 9). As can be seen, a decrease in the shear modulus by a factor of ten decreases the maximum shear stress by a factor of three. However, the use of this approach must be assessed very carefully, since a reduced shear modulus is usually connected with a reduced shear strength.

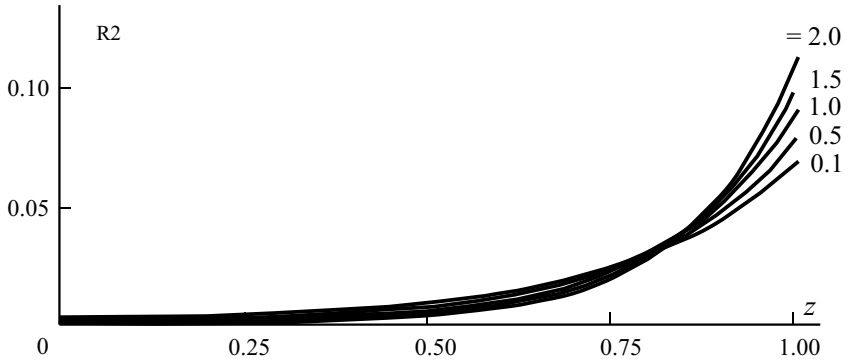

Fig. 12. Shear stresses between the rod and the intermediate cylinder vs. the relative coordinate $\bar{z}$ for different values of . Loading scheme 2. $_L = 30$, $_r = 3.125$, and $_E = 0.01$.

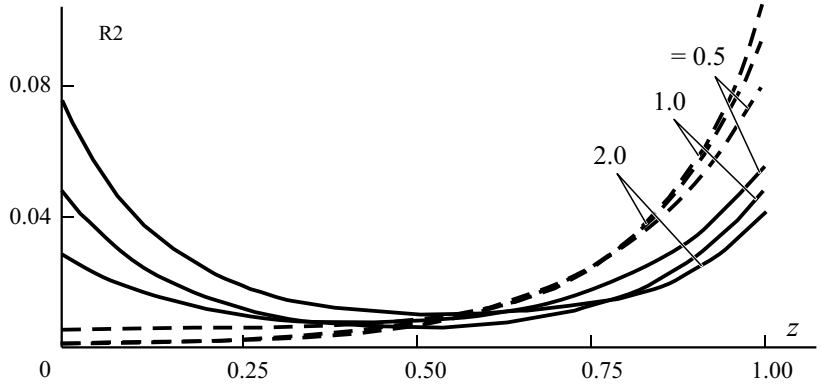

Fig. 13. A comparison of shear-stress distributions between the rod and the intermediate cylinder for loading schemes 1 (—) and 2 (- - -). $_L = 30$, $_r = 3.125$, and $_E = 0.01$.

An increase in the ratio between radii of the intermediate cylinder also decreases the maximum shear stresses at the rod surface (Fig. 10). However, this decrease is limited, because increasing this ratio more than 2.5-3.0 times is ineffective (Fig. 11).

We now proceed to loading scheme 2, which entails an external compressive force on the inner end, , of the sleeve (Fig. 1b). In this case, the shear stresses on the rod surface are described by relation (27). The impact of ($\bar{z} = 1$) on the shear-stress distribution is less evident than in scheme 1 and is opposite to that in scheme 1: greater values of (less stiff sleeves) lead to higher peak shear stresses, which do not change their location ($\bar{z} = 1$), as shown in Fig. 12. Greater values of also lead to greater differences between the stress distributions in schemes 1 and 2 (Fig. 13). It can also be seen that the loading according to scheme 1 significantly decreases the peak shear stress near the inner end of the rod. The fact that the distribution of shear stress depends on the method of loading was noticed in experiments with potted anchors [10] and in pull-out tests of fibers [17].

Next we will consider the case where the external force is applied to a point between ends of the sleeve (scheme 3, Fig. 1c). The relative shear stresses in the regions to the right and left of the applied force are again obtained by transforming Eqs. (21) and (22), respectively. The relative forces $\bar{F}_{\text{Sl},2}$ $F_{\text{Sl},2}/P$ in the sleeve are obtained from Eqs. (23) and (24). In such a loading, one part of the sleeve is compressed and the other one stretched. The relative compressive $\bar{F}_{\text{Sl}}$ and tensile $\bar{F}_{\text{S2}}$ forces created in the rod for loading positions 0 $\bar{l}_1$ 1 ($\bar{l}_1$ l_1/l) are given in Fig. 14. As seen, at certain values of $\bar{l}_1$ (0.78 for $_E$ = 0.01 and 0.935 for $_E = 0.1$), the forces to the left ($\bar{F}_{\text{Sl}} = -0.42$) and right ($\bar{F}_{\text{S2}} = 0.58$) of the load point do not depend on the ra-

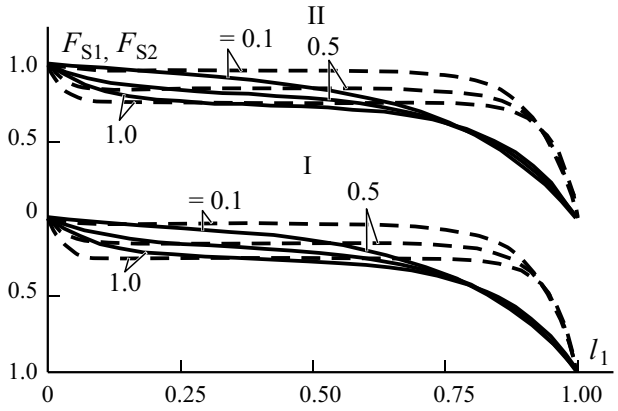

Fig. 14. Normalized longitudinal forces $\bar{F}_{Sl}$ (lower curves) and $\bar{F}_{S2}$ (upper curves) at the load point ($\bar{z} = \bar{l}_1$) vs. the load-point position $\bar{l}_1$ for $_E$ = 0.01 (——) and 0.1(- - -). $_L$ = 30 and $_r$ = 3.125. Loading scheme 3.

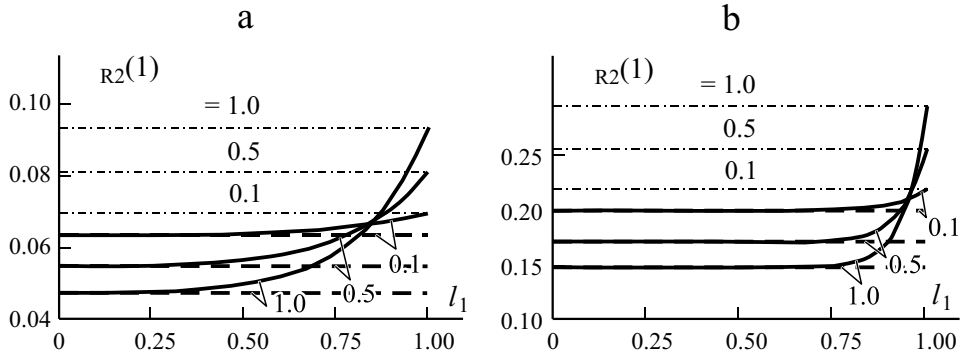

Fig. 15. Shear stresses $\bar{}_{R2}$ ($\bar{z}$ l) on the rod surface vs. the load-point position $\bar{l}_1$ for $_E$ = 0.01 (a) and 0.1 (b). The dashed and dash-dotted lines correspond to the values of $\bar{}_R$ for cases where the external load is applied at $\bar{z}$ 1 ($\bar{l}_1$ = 1); (- - -) and $\bar{z}$ = 0 ($\bar{l}_1$ = 0), respectively. $_L$ = 30 and $_r$ = 3.125.

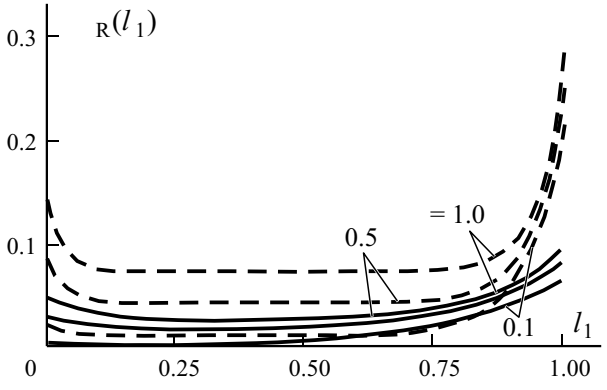

Fig. 16. Relative shear stresses $\bar{}_R$ at $\bar{z} = \bar{l}_1$ on the rod surface vs. the load-point position $\bar{l}_1$ for $_E$ = 0.01 (——) and (- - -). $_L$ = 30 and $_r$ = 3.125.

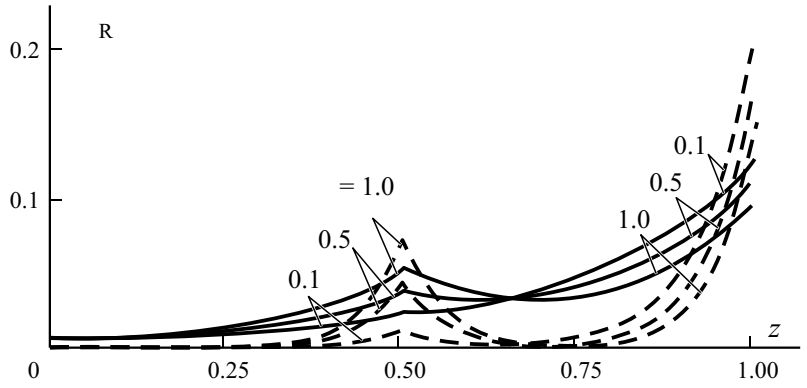

Fig. 17. Distribution of the relative shear stresses $\bar{}_{R1}$ and $\bar{}_{R2}$ along the rod-tendon surface for the case where the load is applied at $\bar{z} = \bar{l}_1 = 0.5$ for $_E = 0.01$ (——) and 0.1 (- - -). $_L = 30$

tio between tensile stiffnesses of the rod and sleeve. It is also seen that the location of the load point when the tensile and compressive forces are equal to half the applied load is about $\bar{l}_1 = 0.83$ at $_E = 0.01$ and about $\bar{l}_1 = 0.95$ at $_E = 0.1$. Thus, by changing the location of the load point or by decreasing the sleeve thickness and making it more compliant, one can significantly increase its longitudinal load-carrying capacity.

The relative peak interfacial shear stress between the rod and pottant (at $\bar{z} = 1$) as a function of location of the load point are presented in Fig. 15a, b. As seen, a shift of the load point from $\bar{z} = 1$ to lower values decreases the shear stresses significantly only for relatively compliant sleeves, whose stiffnesses is of the same order of magnitude as that of the composite rod. There is a wide range of $\bar{l}_1$ within which the location of the load point does not have a noticeable influence on the maximum shear stresses (0 $\bar{l}_1$ 0.5 at $_E = 0.01$ and 0 $\bar{l}_1$ 0.8 at $_E = 0.1$). There also exist locations of the load for which the relation between sleeve and rod stiffnesses does not practically influence the peak interfacial shear stress ($\bar{l}_1$ 0.845 at $_E = 0.01$ and $\bar{l}_1$ 0.95 for at $_E = 0.1$).

The shear stresses on the rod surface at the cross section corresponding to the load point $\bar{z} = \bar{l}_1$ are usually lower than those at the inner end $\bar{z} = 1$ of the sleeve (compare Figs. 15 and 16). This is also clearly seen in Fig. 17, where the distributions of shear stresses along the rod surface are presented for the case where the external force is applied at the midpoint of sleeve length (at $\bar{z} = 0.5$). As may be seen from a comparison with the data presented in Fig. 16, the maximum shear stresses in this case are lower than the maximum shear stresses in the anchor where the sleeve loaded with a compressive force at $\bar{z} = 1$ and are practically equal to those in the sleeve loaded with a tensile force at $\bar{z} = 0$.

Conclusions

The results obtained during the analysis of the model of potted bond-type anchors with a sleeve of constant thickness lead to the following practical conclusions.

1. The compliance of the sleeve significantly affects the shear-stress distribution at the surface of the FRP rod.

2. The effect of compliance of the sleeve depends on the axial location of the external load on the anchor. An increase in the compliance decreases the peak shear stress at the inner end of the rod when the sleeve is loaded with a tensile force at its outer end and increases the peak stress at the inner end of the rod when the sleeve is loaded with a compressive force at its inner end.

3. In all the cases considered, the maximum shear stress is higher when the sleeve is loaded at its inner end.

4. Lengthening the anchor decreases the maximum shear stress to a certain limit. In the cases considered, variations in this stress practically come to a stop as soon as the relative length exceeds the values 25-30.

5. An effective means of reducing the peak shear stress is diminishing the shear modulus of the potted intermediate cylinder. A decrease in the shear modulus by a factor of ten decreases the maximum shear stress by a factor of three.

6. An increase in the ratio between radii of the potted intermediate cylinder also decreases the peak shear stress, but this decrease is limited. Increasing this ratio more than 2.5-3.0 times is ineffective.

7. The load-carrying capacity of the sleeve can be increased by shifting the load point from either end of the sleeve to intermediate sections.

8. Shifting the load point from the inner end of the sleeve to its midpoint decreases the peak shear stress significantly only in the case of relatively compliant sleeves, whose stiffness is of the same order of magnitude as that of the composite rod. There is a wide range of load-point positions within which the location of the point does not have a noticeable influence on the peak shear stress.

Using some modifications of the model proposed, the load-carrying capacity of potted anchors with sleeves of variable thickness, multipotted anchors, and anchors with an elastic friction bond between the pottant and rod will be studied in further investigations.

REFERENCES

1. L. C. Hollaway, "The evolution of and the way forward for advanced polymer composites in civil infrastructure," Construct. Build. Mater., **17**, 365-378 (2003).
2. J. F. Noisterung, "Carbon composites as stay cables for bridges," Appl. Compos. Mater., **7**, 139-150 (2000).
3. A. Mortazavi, "Anchorage and shear strength properties for composite tendons used in earthwork support systems," Construct. Build. Mater., **21**, 109-117 (2007).
4. A. Nanni, C. E. Bakis, E. F. O'Neil, and T. O. Dixon, "Performance of FRP tendon-anchor systems for prestressed concrete structures," PCI J., **41**, 34-44 (1996).
5. B. Zhang, B. Benmonkrane, A. Chennnouf, and P. Mukhopadhyaya, "Tensile behavior of FRP tendons for prestressed ground anchors," J. Compos. Construct., **5**, 85-93 (2001).
6. E. J. Barbero, "Construction," in: S. T. Peters (ed.) Handbook of Composites, Chapman & Hall, London (1998), p. 982-995.
7. H. Nordin, Strengthening Structures with Externally Prestressed Tendons. Literature Review. Technical Report, 06, Lulea University of Technology (2005).
8. B. Zhang, B. Benmokrane, and A. Chennouf, "Prediction of tensile capacity of bond anchorages for FRP tendons," J. Compos. Construct., **4**, 39-47 (May, 2000).
9. F. S. Rostasy and H. Budelmann, "Principles of design of FRP tendons and anchorages for post-tensioned concrete," in: A. Nanni and C. W. Dolan (eds.), Int. Symp. Fibre-Reinforced Plastic Reinforcement for Concrete Structures, 1993, ACI SP 138-38 (1993), pp. 633-649.
10. B. Zhang and B. Benmokrane, "Design and evaluation of a new bond-type anchorage system for fiber reinforced polymer tendons," Can. J. Civ. Eng., **31**, 14-26 (2004).
11. S. Kosaoz, V. A. Samaranayake, and A. Nanni, "Tensile characterization of glass FRP bars," Composites, Pt. B, **36**, 127-134 (2005).
12. B. Benmokrane, H. Xu, and I. Nishizaki, "Aramid and carbon fibre-reinforced plastic prestressed ground anchors and their field applications," Can. J. Civ. Eng., **24**, No. 6, 968-985 (1997).
13. M. A. Erki and S. H. Rizkalla, "Anchorages for FRP reinforcement," ACI Concr. Int., Design Construct., **15**, No. 6, 54-59 (1993).
14. G. G. Portnov and C. E. Bakis, "Analysis of stress concentration during tension of round pultruded composite rods," Compos. Struct., **83**, 100-109 (2008).
15. A. Nairn, "On the use of shear-lag methods for analysis of stress transfer in unidirectional composites," Mech. Mater., **26**, 63-80 (1997).
16. C. Galiotis and A. Paipetis, "Definition and measurement of the shear-lag parameter, , as an index of the stress transfer efficiency in polymer composites," J. Mater. Sci., **33**, 1137-1143 (1998).

17. C. Y. Yue and H. C. Looi, "Factors which influence the reliability of the assessment of interfacial bonding in fibrous composites using the pull-out test," Int. J. Adhes. Adhesiv., **21,** 309-323 (2001).
18. B. Banholzer, W. Brameshuber, and W. Jung, "Analytical simulation of pull-out tests — direct problem," Cem. Concr. Compos., **27**, 93-101 (2005).
19. H. L. Cox, "The elasticity and strength of paper and other fibrous materials," Brit. J. Appl. Phys., **3**, 72-79 (1952).
20. J. A. Nairn and D. A. Mendels, "On the use of planar shear-lag methods for stress-transfer analysis of multilayered composites," Mech. Mater., **33**, 335-362 (2001).
21. R. Tepfers, A Theory of Bond Applied to Overlapped Tensile Reinforcement Splices for Deformed Bars. PhD Thesis, Chalmers University of Technology, Division of Concrete Structures, Goteborg, Sweeden, Publication 73:2 (1973).
22. J. L. Lubkin and E. Reissner, "Stress distribution and design data for adhesive lap joints between circular tubes," Trans. ASME, 1213-1221 (August, 1956).
23. R. D. Adams and N. A. Peppiatt, "Stress analysis of adhesive bonded tubular lap joints" J. Adhes., **9**, 1-18 (1977).
24. C. Lee, M. I. Basci, and L. J. Mignosa, "An elastic-plastic solution for tubular bonded joint under axial load," in: AIAA/ASME/ASCE/AHS/ASC Structures, Structural Dynamics and Materials Conference, 35th, Hilton Head, SC, April 18-20, 1994, Technical Papers, Pt. 5 (a94-23876 06-39), American Institute of Aeronautics and Astronautics, Washington, DC (1994), pp. 2591-2598.
25. A. Al-Mayah, K. Soudki, and A. Plumtree, "Mechanical behavior of CFRP rod anchors under tensile loading," J. Compos. Construct., **5**, 128-135 (2001).
26. M. Keuser, B. Kepp, G. Mehlhorn, and F. Rostasy, "Nonlinear static analysis of end-fittings for GFRP-prestressing rods," Comput. Struct., **17**, Nos. 5-6, 719-730 (1983).
27. M. A. Koltunov, J. N. Vasiliev, and V. A. Chernih, Elasticity and Strength of Cylindrical Bodies [in Russian], Visshaya Shkola, Moscow (1975).
28. K. V. Soljanic-Krassa, Axisymmetric Problem in the Theory of Elasticity [in Russian], Stroiizdat, Moscow (1987).
29. R. D. Adams, J. Comyn, and W. C. Wake, Structural Adhesive Joints in Engineering, Chapman & Hall (1997).
30. Z. Tian, F. Zhao, and Q. Yang, "Straight free-edge effects in laminated composites," Finite Elem. Anal. Design, **41**, 1-14 (2004).
31. A. G. Magalhaes, M. F. S. F. de Moura, and J. P. M. Goncalves, "Evaluation of stress concentration effects in single-lap joints of laminate composite materials," Int. J. Adhes. Adhesiv., **25**, 313-319 (2005).
32. C. E. Bakis and T. E. Boothby, "Experimental evaluation of mechanical and thermal properties of carbon and aramid FRP tendons," in: A. H. Hosny, A. Abdelrahman, and A. W. El-Ghandour (eds.), Proc. Y Middle East Symp. Struct. Compos. Infrastructure Applications — Innovations and Applications, Paper VII-1, Egyptian Soc. Eng., Cairo (2008), p. 10.